Supporting information for: Application of the Peng-Robinson equation of state to energetic materials RDX and TNT: pure components, liquid mixtures, and solid mixtures

Philip C. Myint,*,† Matthew A. McClelland,‡ and Albert L. Nichols III‡

†*Design Physics Division, Lawrence Livermore National Laboratory, Livermore, CA, USA*

‡*Materials Science Division, Lawrence Livermore National Laboratory, Livermore, CA, USA*

E-mail: myint1@llnl.gov

Outline of the Peng-Robinson equation of state

The Peng-Robinson equation of state (EOS)[S1] — like other cubic EOS and many other types of equations of state — may be expressed in terms of a departure function, which is also called a residual or a residual function. A departure function is defined as the difference in some property of a substance, which can be either a pure component or a mixture, and that same property of the substance if it were to exist as an ideal gas at the same conditions. If the total number of moles of the substance is N and its volume is V so that its molar density ρ is N/V, the Peng-Robinson equation of state's expression[S2,S3] for the Helmholtz

energy departure function F^{depart} is

$$\frac{F^{\text{depart}}}{NRT} = -\ln(1-b\rho) - \frac{a}{2\sqrt{2}bRT}\ln\left[\frac{1+(1+\sqrt{2})b\rho}{1+(1-\sqrt{2})b\rho}\right]. \tag{1}$$

Here, R is the gas constant, and T is the temperature. Intermolecular interactions and non-zero molecular volumes are represented by the parameters a and b, respectively. In practice, these parameters serve as adjustable variables that are fitted to experimental data. For mixtures, a and b are computed from the pure-component parameters a_i and b_i using one of a number of different mixing rules.[S4–S7] In this study we use the standard van der Waals mixing rules, which are the most commonly employed set of schemes and which compare favorably with more complicated mixing rules even at pressures higher than 1000 bar.[S5] The van der Waals mixing rules for a mixture of c components are

$$a = \sum_{i=1}^{c}\sum_{j=1}^{c} z_i z_j a_{ij}, \tag{2}$$

$$a_{ij} = (1-k_{ij})a_i^{1/2}a_j^{1/2}, \tag{3}$$

$$b = \sum_{i=1}^{c} z_i b_i, \tag{4}$$

where z_i is the mole fraction of component i, and k_{ij} is the binary interaction coefficient between components i and j. These coefficients are defined so that $k_{ii} = 0$ and $k_{ij} = k_{ji}$ is generally non-zero for all i, j.

All of the thermodynamic property predictions of the Peng-Robinson EOS (e.g., density, equilibrium composition, heat capacity) can be derived from (1). For the purposes of completeness and ease of reference, we present the most fundamental equations in this section. We give expressions for other properties in the main text as needed. We start with the

pressure P, which is related to the Helmholtz energy through

$$P = -\left(\frac{\partial F}{\partial V}\right)_{T,\mathbf{n}} = \frac{\rho^2}{N}\left(\frac{\partial F}{\partial \rho}\right)_{T,\mathbf{z}},$$

where $\mathbf{z} = (z_1, z_2, \ldots, z_i, \ldots, z_c)$ represents the component mole fractions, and $\mathbf{n} = N\mathbf{z}$. Applying the indicated derivative to (1) yields

$$P = \frac{\rho RT}{1 - b\rho} - \frac{a\rho^2}{1 + 2b\rho - (b\rho)^2}. \tag{5}$$

Dividing both sides of (5) by ρRT, the compressibility factor $Z = P/\rho RT$ is given by

$$Z = \frac{1}{1 - b\rho} - \frac{1}{RT}\frac{a\rho}{1 + 2b\rho - (b\rho)^2}. \tag{6}$$

Let us define new variables A and B that are dimensionless analogues of a and b, respectively:

$$A(T, P, \mathbf{z}) = \frac{aP}{R^2T^2}, \tag{7}$$

$$B(T, P, \mathbf{z}) = \frac{bP}{RT}. \tag{8}$$

Combining (6)–(8), we find that Z satisfies the cubic polynomial equation

$$Z^3 + (B - 1)Z^2 + (A - 3B^2 - 2B)Z + B(B^2 + B - A) = 0. \tag{9}$$

We substitute (7) and (8) into (1) to obtain

$$\frac{F^{\text{depart}}}{NRT} = \ln\left(\frac{Z}{Z - B}\right) - \frac{A}{2\sqrt{2}B}\ln\left[\frac{Z + (1 + \sqrt{2})B}{Z + (1 - \sqrt{2})B}\right]. \tag{10}$$

Phase equilibria calculations require the computation of chemical potentials, which in practice means the computation of fugacities.[S8] Since the Peng-Robinson EOS's expres-

sions for the thermodynamic properties are all ultimately derived from a departure function [either (1) or its alternative form (10)], it is more natural to work directly with fugacity coefficients rather than with fugacities. The fugacity coefficient $\phi_i = \phi_i(T, P, \mathbf{z})$ is defined as the ratio f_i/z_iP, where $f_i = f_i(T, P, \mathbf{z})$ is the fugacity of component i in a real (non-ideal) mixture at the conditions $(T, P, \mathbf{z})$, and z_iP is the fugacity of i if the mixture were to exist as an ideal gas at the same conditions. The chemical potential μ_i in the real mixture is related to its value μ_i^{ig} in the hypothetical ideal gas mixture according to

$$\mu_i(T, P, \mathbf{z}) = \mu_i^{\text{ig}}(T, P, \mathbf{z}) + RT \ln \phi_i(T, P, \mathbf{z}). \tag{11}$$

By taking the appropriate composition derivative of (10) it can be shown (see, for example, Elliott and Lira[S2] for details on the derivation) that

$$\begin{aligned} \ln \phi_i(T, P, \mathbf{z}) = &- \ln (Z - B) + \frac{B_i}{B}\left(\frac{B}{Z - B} - \frac{AZ}{Z^2 + 2BZ - B^2}\right) \\ &- \frac{A}{2\sqrt{2}B}\left(\frac{2\sum_{j=1}^{c} z_j A_{ij}}{A} - \frac{B_i}{B}\right) \ln\left[\frac{Z + (1 + \sqrt{2})B}{Z + (1 - \sqrt{2})B}\right], \end{aligned} \tag{12}$$

where

$$B_i = \frac{b_i P}{RT},$$

$$A_{ij} = \frac{a_{ij} P}{R^2 T^2} = \frac{(1 - k_{ij}) a_i^{1/2} a_j^{1/2} P}{R^2 T^2}.$$

For a pure component, (11) and (12) simplify to

$$\mu_i(T, P) = \mu_i^{\text{ig}}(T, P) + RT \ln \phi_i(T, P), \tag{13}$$

$$\ln \phi_i(T, P) = - \ln (Z - B) + \left(\frac{B}{Z - B} - \frac{AZ}{Z^2 + 2BZ - B^2}\right) - \frac{A}{2\sqrt{2}B} \ln\left[\frac{Z + (1 + \sqrt{2})B}{Z + (1 - \sqrt{2})B}\right]. \tag{14}$$

Results with temperature-dependent b_i

In addition to developing a Peng-Robinson EOS model with constant b_i, which is the subject of the main text, we have also developed a model with temperature-dependent b_i for solid RDX, solid TNT, and liquid TNT. We have stated in the main text that the results between the two models are comparable; each offers its own advantages. The temperature dependence allows for a direct fit to volumetric data at atmospheric pressure. As we discuss later in this section, it also generally improves the heat capacity predictions depicted in Figures 4 and 10 of the main text, but likely produces less accurate results for the liquid RDX heat capacity (though experimental data is not available to verify this). Temperature-dependent b_i also lead to modest changes in the melting behavior of TNT at pressures above 1000 bar. This section briefly describes how we have formulated the temperature dependence. We then compare the results between this model and the one with constant b_i for all compounds. For the sake of brevity, we focus only on properties where there are noticeable differences between the two models. For example, we neglect the bulk modulus K_T in this section because the results are virtually identical to those illustrated in Figure 2.

By fitting a_i and b_i to vapor pressure data and atmospheric-pressure volumetric data,[S9–S12] we are able to represent $a_i(T)$ and $b_i(T)$ for solid RDX, solid TNT, and liquid TNT as

$$a_i(T) = a_{1,i}T + a_{0,i}, \tag{15}$$

$$b_i(T) = b_{3,i}T^3 + b_{2,i}T^2 + b_{1,i}T + b_{0,i}. \tag{16}$$

Tables S1 and S2 list the values of the coefficients used in these equations. Once the critical temperature and pressure of TNT have been accurately determined, one can employ cubic splines to extend (15) and (16) for liquid TNT up to the critical point so that they are compatible with Equations (1) and (2), respectively, in the main text. Figure S1 compares

the melting behavior of pure TNT between the two models. The normal melting temperature is slightly lower in the constant b_i model (353.65 K vs. 353.66 K). At the resolution of the figure, the difference in T_{melt} becomes discernible — though still small — only for pressures greater than 1000 bar. The two melting curves diverge by less than 2% even at 2500 bar.

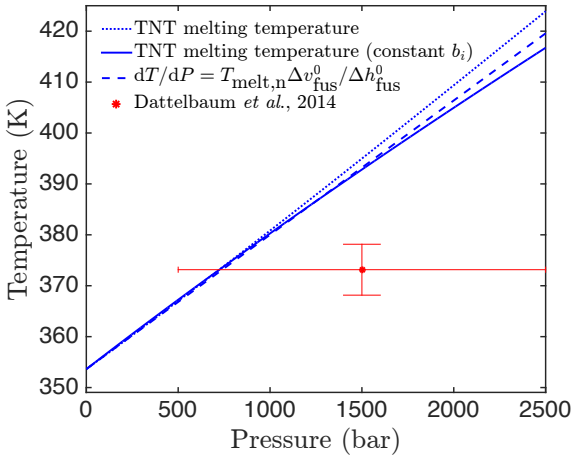

Figure S1: The melting temperature T_{melt} of TNT vs. pressure. The T_{melt} predicted by the constant b_i model is less than that of the temperature-dependent b_i model (dotted line) at all pressures, though the deviation remains small (less than 2%) even at 2500 bar.

Table S1: Coefficients for calculating a_i in (15). The units of these coefficients are such that a_i has units of $\text{L}^2\cdot\text{bar/mole}^2$.

Compound	$a_{1,i}$	$a_{0,i}$
Solid RDX	-0.2845952	249.6884446
Solid TNT	-0.3879503	258.0588946
Liquid TNT	-0.2382614	217.4506615

Table S2: Coefficients for calculating b_i in (16). The units of these coefficients are such that b_i has units of L/mole.

Compound	$b_{3,i} \times 10^{10}$	$b_{2,i} \times 10^{8}$	$b_{1,i} \times 10^{6}$	$b_{0,i}$
Solid RDX	-1.2225317	6.5137031	-6.2674083	0.1182848
Solid TNT	0	-0.14676838	-11.0518361	0.1346203
Liquid TNT	0	-15.1025226	153.5176465	0.1092381

Figure S2 presents constant-pressure molar heat capacity c_P predictions. The temperature-dependent b_i clearly lead to better results for solid RDX, but they do not conclusively improve

the accuracy for TNT. In fact, one could argue that the c_P predictions of solid TNT are likely to be better with the constant b_i model since they lie closer to the middle, rather than the lower edge, of the experimental range. Because the solid RDX property predictions between the two formulations are a little different, the liquid RDX parameters must be subsequently adjusted to obtain the same values for $T_{\mathrm{melt,n}}$, $\Delta v^0_{\mathrm{fus}}$, and $\Delta h^0_{\mathrm{fus}}$ presented in Table 2. By following the procedure described in the Liquid RDX Section, we match these results if $b_{\mathrm{RDX}} = 0.1197530$ L/mole, and a_{RDX} in units of $\mathrm{L^2{\cdot}bar/mole^2}$ is given by

$$a_{\mathrm{RDX}}(T) = \exp(a_{1,\mathrm{RDX}}T + a_{0,\mathrm{RDX}}), \tag{17}$$

where $a_{1,\mathrm{RDX}} = -1.0291542 \times 10^{-3}$ $\mathrm{K^{-1}}$, and $a_{0,\mathrm{RDX}} = 5.2479336$.

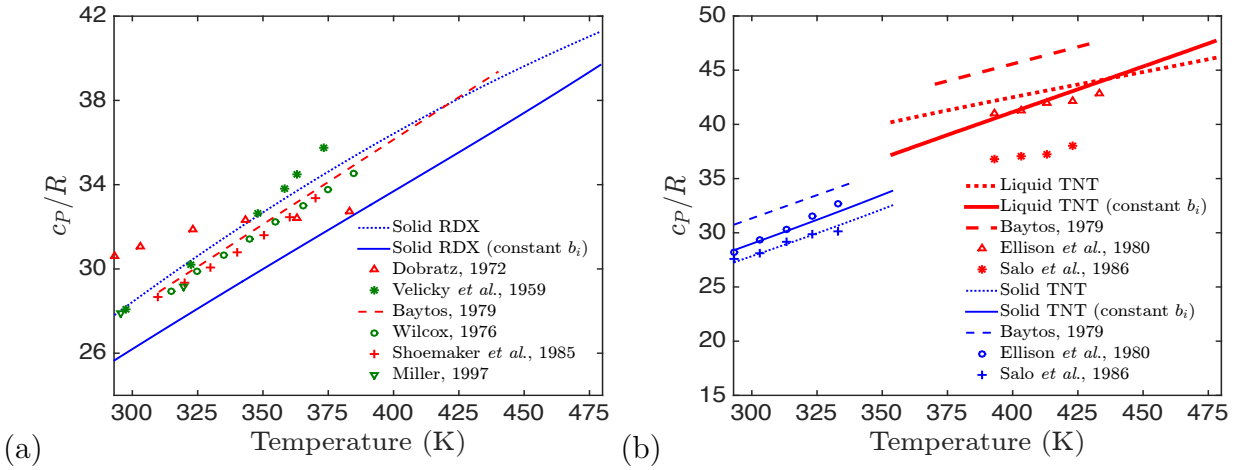

Figure S2: Constant-pressure molar heat capacity c_P of (a) RDX and (b) TNT vs. temperature at atmospheric pressure. Representative experimental values are included for comparison.[S13–S20] The results are non-dimensionalized by R. The average absolute deviations (AADs) between our constant b_i (temperature-dependent b_i) predictions and Baytos' linear fits to temperature[S15] are 6.7% (1.2%), 7.0% (10.7%), and 9.8% (6.8%) for solid RDX, solid TNT, and liquid TNT, respectively. The AADs compared to the results of Ellison *et al.*[S19] are 1.1% (4.8%) and 1.4% (3.0%) for solid TNT and liquid TNT, respectively.

A potential drawback of this model is that the liquid RDX heat capacity is a few percent lower than that of solid RDX at $T_{\mathrm{melt,n}}$ ($40.1R$ vs. $41.2R$ at this temperature). This is minor compared to the 20–30% lower liquid c_P values we have obtained in our earlier efforts to

calculate a_{RDX} and b_{RDX} from theoretical predictions of the critical temperature (see the Liquid RDX Section for more details), but is nonetheless physically unrealistic. We have found that c_P of the liquid is sensitive to Δh^0_{fus}. By selecting Δh^0_{fus} to be 30.0 kJ/mole (but keeping the same $T_{\text{melt,n}}$ and $\Delta v^0_{\text{fus}}/\Delta h^0_{\text{fus}}$ ratio), which is a little below the experimental range of 30.7–35.7 kJ/mole shown in Table 2, we obtain a liquid RDX heat capacity of $41.4R$ at $T_{\text{melt,n}}$ (compared to $41.2R$ for solid RDX). These results can be obtained if $b_{\text{RDX}} =$ 0.1194051 L/mole with $a_{1,\text{RDX}} = -1.1740738 \times 10^{-3}$ K^{-1} and $a_{0,\text{RDX}} = 5.3145238$ in (17).

We model RDX/TNT mixtures by combining the just aforementioned liquid RDX parameters with parameters for the other pure components through the van der Waals mixing rules in (2)–(4). This involves selecting the binary interaction coefficients $k^l_{\text{RDX-TNT}}$ and $k^s_{\text{RDX-TNT}}$ to reproduce the experimental solubility measurements of Campbell and Kushnarov.[S21] We treat $k^s_{\text{RDX-TNT}}$ as a constant, but model $k^l_{\text{RDX-TNT}}(T)$ according to

$$k^l_{\text{RDX-TNT}}(T) = k_3(T - T_{\text{eutectic,n}})^3 + k_2(T - T_{\text{eutectic,n}})^2 + k_1(T - T_{\text{eutectic,n}}) + k_0, \qquad (18)$$

where $k^s_{\text{RDX-TNT}}$ and k_0 are listed in Table S3, $k_1 = 4.413 \times 10^{-4}$, $k_2 = -5.062 \times 10^{-6}$, and $k_3 = -6.958 \times 10^{-9}$. The AAD and root mean square deviation (RMSD) between our results and Campbell and Kushnarov's data for the right branch of the liquidus curve are 3.89% and 0.0106, respectively. Comparing the values in Table S3 to those in Table 3, we see that the temperature-dependent b_i model predicts higher-purity solid mixtures at the eutectic temperature $T_{\text{eutectic,n}}$. However, these differences are not significant (i.e., the phase diagram at $P = 1$ bar is essentially identical to Figure 5), especially given the absence of data for the solid-phase curves. The phase diagrams at higher pressures also appear similar to the results presented in the main text; there are small differences due to, for example, the deviation in the pure TNT melting curves (Figure S1), but these differences are not readily noticeable at the resolution of Figure 6. Figure S3 shows that the temperature-dependent b_i model predicts

heat capacities for Composition B-3 (Comp B-3) that match the experimental data more closely. At temperatures below $T_{\text{eutectic,n}}$, the improved agreement is largely a consequence of the more accurate predictions for solid RDX. Comp B-3 is at least partially liquid above $T_{\text{eutectic,n}}$ (see Figure 8). Some of the behavior at these temperatures (such as the jump in c_p at $T_{\text{eutectic,n}}$ and the faster rise of the constant b_i curve) can be reasoned from the TNT results in Figure S2. However, since the liquid phase contains a significant amount of both RDX and TNT so that non-ideal mixing effects may be prominent, we cannot fully explain the Comp B-3 heat capacity results from the behavior of the pure components alone.

Table S3: Results for our temperature-dependent b_i model at the eutectic temperature $T_{\text{eutectic,n}}$ at $P = 1$ bar. The compositions of the three phases listed here are expressed in terms of the RDX mole fraction. The value of $T_{\text{eutectic,n}}$ itself and the liquid composition are obtained from Campbell and Kushnarov,[S21] while the other four quantities are calculated by solving the conditions for equilibrium in Equation (21) of the main text.

$T_{\text{eutectic,n}}$ (K)	$k^l_{\text{RDX-TNT}}$	$k^s_{\text{RDX-TNT}}$	Liquid	RDX-rich solid	TNT-rich solid
351.45	-0.0115103	0.0945402	0.05107	0.99503	0.00871

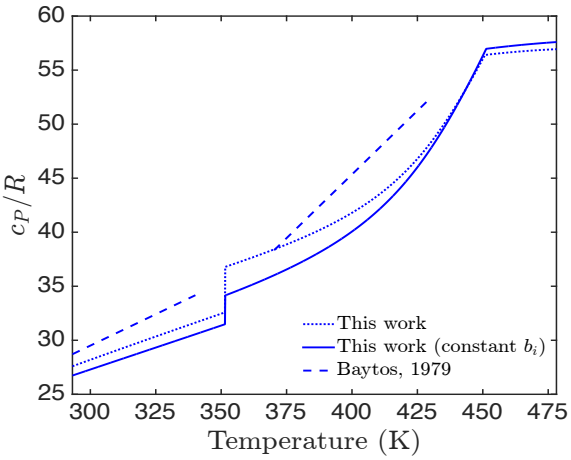

Figure S3: Comparison of our predictions for the Comp B-3 constant-pressure molar heat capacity c_P at atmospheric pressure with experimental data from Baytos.[S15] He has fit his data to linear functions of temperature in two regimes: one below the eutectic temperature $T_{\text{eutectic,n}}$ and the other above $T_{\text{eutectic,n}}$. The average absolute deviations between his linear fits in these two regimes and our constant b_i (temperature-dependent b_i) results are 8.8% (5.7%) and 10.3% (6.5%), respectively.

Tables

Table S4: Values of A_{vap} and B_{vap} selected to calculate the vapor pressure with the Clausius-Clapeyron equation (9) of the main text. The values for solid RDX are from Östmark *et al.*,[S22] while those for solid and liquid TNT are from Edwards.[S23] As explained in the main text, we have slightly increased A_{vap} for solid TNT from the value presented by Edwards (14.34) so that the normal melting point temperature of TNT lies in the range 353–354 K commonly cited in the literature.[S21,S24–S27]

Compound	A_{vap}	B_{vap} (K)	Units of P^0
Solid RDX	13.79	6637	mm Hg
Solid TNT	14.35	6180	cm Hg
Liquid TNT	10.90	4960	cm Hg

Table S5: The coefficients obtained by fitting Equation (18) of the main text to the quantum calculations of Osmont *et al.*,[S28] where the units of the ideal gas heat capacity c_P^{ig} are kJ·mole^{-1}·K^{-1}. This quantity is used in Equation (17) of the main text to find the constant-pressure molar heat capacity c_P.

Compound	$c_3 \times 10^{10}$	$c_2 \times 10^7$	$c_1 \times 10^4$	c_0
RDX	2.0985786	-7.2921143	9.5011103	-0.0192740
TNT	1.8156981	-6.7242857	9.0248654	0.0045077

References

(S1) Peng, D.-Y.; Robinson, D. B. A new two-constant equation of state. *Ind. Eng. Chem. Fundamen.* **1976**, *15*, 59–64, DOI: 10.1021/i160057a011.

(S2) Elliott, J. R.; Lira, C. T. *Introductory Chemical Engineering Thermodynamics*, 1st ed.; Prentice Hall, Upper Saddle River, 1999.

(S3) Myint, P. C.; Hao, Y.; Firoozabadi, A. *The CPA equation of state and an activity coefficient model for accurate molar enthalpy calculations of mixtures with carbon dioxide and water/brine*; Technical Report LLNL-TR-672077, Lawrence Livermore National

Laboratory, 2015; 43 pp., DOI: 10.2172/1194030, https://e-reports-ext.llnl.gov/pdf/790891.pdf.

(S4) Huron, M.-J.; Vidal, J. New mixing rules in simple equations of state for representing vapour-liquid equilibria of strongly non-ideal mixtures. *Fluid Phase Equilibr.* **1979**, *3*, 255–271, DOI: 10.1016/0378-3812(79)80001-1.

(S5) Shibata, S. K.; Sandler, S. I. Critical evaluation of equation of state mixing rules for the prediction of high-pressure phase equilibria. *Ind. Eng. Chem. Res.* **1989**, *28*, 1893–1898, DOI: 10.1021/ie00096a024.

(S6) Michelsen, M. L. A modified Huron-Vidal mixing rule for cubic equations of state. *Fluid Phase Equilibr.* **1990**, *60*, 213–219, DOI: 10.1016/0378-3812(90)85053-D.

(S7) Mathias, P. M.; Klotz, H. C.; Prausnitz, J. M. Equation-of-state mixing rules for multicomponent mixtures: the problem of invariance. *Fluid Phase Equilibr.* **1991**, *67*, 31–44, DOI: 10.1016/0378-3812(91)90045-9.

(S8) Prausnitz, J. M.; Lichtenthaler, R. N.; Gomes de Azevedo, E. *Molecular Thermodynamics of Fluid-Phase Equilibria*, 3rd ed.; Prentice Hall, Upper Saddle River, 1999.

(S9) Sun, J.; Shu, X.; Liu, Y.; Zhang, H.; Liu, X.; Jiang, Y.; Kang, B.; Xue, C.; Song, G. Investigation on the thermal expansion and theoretical density of 1,3,5-trinitro-1,3,5-triazacyclohexane. *Propell. Explos. Pyrot.* **2011**, *36*, 341–346, DOI: 10.1002/prep.201000026.

(S10) Cady, H. H.; Rogers, W. H. *Enthalpy, density, and coefficient of thermal expansion of TNT*; Technical Report LA-2696, Los Alamos National Laboratory, 1962; 16 pp., http://catalog.hathitrust.org/Record/012213646.

(S11) Vrcelj, R. M.; Sherwood, J. N.; Kennedy, A. R.; Gallagher, H. G.; Gelbrich, T. Polymorphism in 2-4-6 trinitrotoluene. *Crystal Growth & Design* **2003**, *3*, 1027–1032, DOI: 10.1021/cg0340704.

(S12) Rosen, J. M.; Sickman, D. V.; Morris, W. W. *The melting behavior of TNT*; Technical Report 6146, U.S. Naval Ordinance Laboratory, 1959; `http://www.dtic.mil/dtic/tr/fulltext/u2/309257.pdf`.

(S13) Dobratz, B. M. *Properties of chemical explosives and explosive simulants*; Technical Report UCRL-51319, Lawrence Livermore National Laboratory, 1972; 334 pp., DOI: 10.2172/4285272, `http://www.osti.gov/scitech/biblio/4285272`.

(S14) Velicky, R.; Lenchitz, C.; Beach, W. *Enthalpy change, heat of fusion, and specific heat of basic explosives*; Technical Report 2504, Picatinny Arsenal, Dover, New Jersey, 1959.

(S15) Baytos, J. F. *Specific heat and thermal conductivity of explosives, mixtures, and plastic-bonded explosives determined experimentally*; Technical Report LA-8034-MS, Los Alamos National Laboratory, 1979; `http://www.osti.gov/scitech/biblio/5913065`.

(S16) Wilcox, J. D. Differential scanning calorimeter methods in the determination of thermal properties of explosives. M.Sc. thesis, Air Force Institute of Technology, Air University, Wright-Patterson Air Force Base, Ohio, 1976; GAW/ME/67B-3.

(S17) Shoemaker, R. L.; Stark, J. A.; Koshigoe, L. G.; Taylor, R. E. In *Thermal Conductivity 18*, 1st ed.; Ashworth, T., Smith, D. R., Eds.; Springer US, New York, 1985; Chapter 22: Thermophysical Properties of Propellants, pp 199–211, DOI: 10.1007/978-1-4684-4916-7.

(S18) Miller, M. S. *Thermophysical properties of RDX*; Technical Report ARL-TR-1319, Army Research Laboratory, Aberdeen Proving Ground, Maryland, 1997.

(S19) Ellison, D. S.; Alcorn, R. A.; Neal, E. Effects of thermal cycling on trinitrotoluene and tritonal explosive compositions. *J. Hazard Mater.* **1980**, *4*, 57 – 75, DOI: 10.1016/0304-3894(80)80023-9.

(S20) Salo, J.; Cichinski, C.; Carignan, Y.; Turngren, E. Thermodynamic properties of energetic materials. III. Heat capacity of trinitrotoluene (TNT). 13$^{\text{th}}$ Symposium on Explosives and Pyrotechnics, Hilton Head Island, SC, USA. 1986; pp I–21 – I–24.

(S21) Campbell, A. N.; Kushnarov, H. A. A study of systems involving trinitrotoluene, RDX, NENO, and dinitrobenzene, with particular reference to the composition of the binary eutectics. *Can. J. Res.* **1947**, *25*, 216–227, DOI: 10.1139/cjr47b-025.

(S22) Östmark, H.; Wallin, S.; Ang, H. G. Vapor pressure of explosives: A critical review. *Propell. Explos. Pyrot.* **2012**, *37*, 12–23, DOI: 10.1002/prep.201100083.

(S23) Edwards, G. The vapour pressure of 2:4:6-trinitrotoluene. *Trans. Faraday Soc.* **1950**, *46*, 423–427, DOI: 10.1039/TF9504600423.

(S24) Parker, R. P.; Thorpe, B. W. *The phase diagram of the RDX/TNT system*; Technical Note No. 140, Department of Supply, Australian Defence Scientific Service, Defence Standards Laboratories, 1970; 10 pp.

(S25) Dobratz, B. M.; Crawford, P. C. *LLNL Explosives Handbook: Properties of Chemical Explosives and Explosive Simulants*; Lawrence Livermore National Laboratory, 1985.

(S26) Miller, G. R.; Garroway, A. N. *A review of the crystal structures of common explosives. Part 1: RDX, HMX, TNT, PETN, and Tetryl*; Technical Report NRL/MR/6120–

01-8585, U.S. Naval Research Laboratory, 2001; http://www.dtic.mil/dtic/tr/fulltext/u2/a396646.pdf.

(S27) Dattelbaum, D. M.; Chellappa, R. S.; Bowden, P. R.; Coe, J. D.; Margevicius, M. A. Chemical stability of molten 2,4,6-trinitrotoluene at high pressure. *Appl. Phys. Lett.* **2014**, *104*, 021911, DOI: 10.1063/1.4860395.

(S28) Osmont, A.; Catoire, L.; Gökalp, I.; Yang, V. Ab initio quantum chemical predictions of enthalpies of formation, heat capacities, and entropies of gas-phase energetic compounds. *Combust. Flame* **2007**, *151*, 262 – 273, DOI: 10.1016/j.combustflame.2007.05.001.